Generation of polarization-entangled photon pairs in a Bragg reflection waveguide

A. Vallés,[1,*] M. Hendrych,[1] J. Svozilík,[1,2] R. Machulka,[2] P. Abolghasem,[3] D. Kang,[3] B. J. Bijlani,[3] A. S. Helmy,[3] and J. P. Torres[1,4]

[1] *ICFO-Institut de Ciències Fotòniques, Mediterranean Technology Park, Av. Carl Friedrich Gauss 3, 08860 Castelldefels, Barcelona, Spain*

[2] *RCPTM, Joint Laboratory of Optics PU and IP AS CR, 17. listopadu 12, 771 46 Olomouc, Czech Republic*

[3] *Edward S. Rodgers Department of Electrical and Computer Engineering, University of Toronto, 10 Kings College road, Toronto, Ontario M5S3G4, Canada*

[4] *Department of Signal Theory and Communications, Universitat Politècnica de Catalunya, Jordi Girona 1-3, Campus Nord D3, 08034 Barcelona, Spain*

adam.valles@icfo.es

Abstract: We demonstrate experimentally that spontaneous parametric down-conversion in an $Al_xGa_{1-x}As$ semiconductor Bragg reflection waveguide can make for paired photons highly entangled in the polarization degree of freedom at the telecommunication wavelength of 1550 nm. The pairs of photons show visibility higher than 90% in several polarization bases and violate a Clauser-Horne-Shimony-Holt Bell-like inequality by more than 3 standard deviations. This represents a significant step toward the realization of efficient and versatile self pumped sources of entangled photon pairs on-chip.

OCIS codes: (190.4410) Nonlinear optics, parametric processes; (270.0270) Quantum optics.

References and links

1. M. A. Nielsen and I. L. Chuang, *Quantum Computation and Quantum Information*, (Cambridge University Press, 2000).
2. D. Bouwmeester, A. K. Ekert and A. Zeilinger eds., *The Physics of Quantum Information*, (Springer Verlag, 2000).
3. E. Nagali, F. Sciarrino, F. De Martini, L. Marrucci, B. Piccirillo, E. Karimi, and E. Santamato, "Quantum Information Transfer from Spin to Orbital Angular Momentum of Photons," Phys. Rev. Lett. **103**, 013601 (2009).
4. J. P. Torres, K. Banaszek, and I. A. Walmsley, "Engineering nonlinear optic sources of photonic entanglement," Prog. Optics **56**, 227–331 (2011).
5. F. Steinlechner, P. Trojek, M. Jofre, H. Weier, D. Perez, T. Jennewein, R. Ursin, J. Rarity, M. W. Mitchell, J. P. Torres, H. Weinfurter, and Valerio Pruneri, "A high-brightness source of polarization-entangled photons optimized for applications in free space," Opt. Express **20**, 9640–9649 (2012).
6. K. Banaszek, A. U'Ren, and I. A. Walmsley, "Generation of correlated photons in controlled spatial modes by downconversion in nonlinear waveguides," Opt. Lett. **26**, 1367–1369 (2001).
7. M. Fiorentino, S. Spillane, R. G. Beausoleil, T. D. Roberts, P. Battle, and M. W. Munro, "Spontaneous parametric down-conversion in periodically poled KTP waveguides and bulk crystals," Opt. Express **15**, 7479–7488 (2007).
8. A. S. Helmy, B. Bijlani, and P. Abolghasem, "Phase matching in monolithic Bragg reflection waveguides," Opt. Lett. **32**, 2399–2401 (2007).
9. P. Abolghasem, J. Han, B. J. Bijlani, A. Arjmand, and A. S. Helmy, "Continuous-wave second harmonic generation in Bragg reflection waveguides," Opt. Express **17**, 9460–9467 (2009).
10. J. Han, P. Abolghasem, D. Kang, B. J. Bijlani, and A. S. Helmy, "Difference-frequency generation in AlGaAs Bragg reflection waveguides," Opt. Lett. **35**, 2334–2336 (2010).

#186956 - $15.00 USD Received 13 Mar 2013; revised 12 Apr 2013; accepted 12 Apr 2013; published 26 Apr 2013

11. R. Horn, P. Abolghasem, B. J. Bijlani, D. Kang, A. S. Helmy, and G. Weihs, "Monolithic Source of Photon Pairs," Phys. Rev. Lett. **108**, 153605 (2012).
12. B. J. Bijlani and A. S. Helmy,"Bragg reflection waveguide diode lasers," Opt. Lett. **34**, 3734–3736 (2009).
13. B. J. Bijlani, P. Abolghasem, A. Reijnders, and A. S. Helmy, "Intracavity Parametric Fluorescence in Diode Lasers," in *CLEO: 2011 Postdeadline Papers* (Optical Society of America, Washington, DC, 2011), Report No. PDPA3.
14. P. Abolghasem, J. Han, D. Kang, B. J. Bijlani and A. S. Helmy, "Monolithic Photonics Using Second-Order Optical Nonlinearities in Multilayer-Core Bragg Reflection Waveguides," IEEE J. Selected Topics Quantum Electron. **2**, 812–825 (2012).
15. A. S. Helmy, "Phase matching using Bragg reflection waveguides for monolithic nonlinear optics applications," Opt. Express **14**, 1243–1252 (2006).
16. P. Abolghasem, M. Hendrych, X. Shi, J. P. Torres, and A. S. Helmy, "Bandwidth control of paired photons generated in monolithic Bragg reflection waveguides," Opt. Lett. **34**, 2000–2002 (2009).
17. J. Svozilík, M. Hendrych, A. S. Helmy, and J. P. Torres, "Generation of paired photons in a quantum separable state in Bragg reflection waveguides," Opt. Express, **19**, 3115–3123 (2011).
18. J. F. Clauser, M. A. Horne, A. Shimony, and R. A. Holt, "Proposed Experiment to Test Local Hidden-Variable Theories," Phys. Rev. Lett. **23**, 880 (1969).
19. N. Gisin, "Bell's inequality holds for all non-product states," Phys. Lett. A **154**, 201–202 (1991).
20. A. Fine, "Hidden Variables, Joint Probability, and the Bell Inequalities," Phys. Rev. Lett. **48**, 291 (1982).
21. N. Matsuda, H. Le Jeannic, H. Fukuda, T. Tsuchizawa, W. J. Munro, K. Shimizu, K. Yamada, Y. Tokura, and H. Takesue," A monolithically integrated polarization entangled photon pair source on a silicon chip," Sci. Rep. **2**, 817 (2012).
22. A. Orieux, A. Eckstein, A. Lemaitre, P. Filloux, I. Favero, G. Leo, T. Coudreau, A. Keller, P. Milman, and S. Ducci, "Bell states generation on a III-V semiconductor chip at room temperature," arXiv:1301.1764 (2013).
23. P. Abolghasem, J. Han, B. J. Bijlani, A. Arjmand A. S. Helmy, "Highly efficient second-harmonic generation in monolithic matching layer enhanced $Al_xGa_{1-x}As$ Bragg reflection waveguides," IEEE Photon. Tech. Lett. **21**, 1462 (2009).
24. S. V. Zhukovsky, L. G. Helt, D. Kang, P. Abolghasem, A. S. Helmy, and J. E. Sipe, "Generation of maximally-polarization-entangled photons on a chip," Phys. Rev. A **85**, 013838 (2012).
25. The chosen polarization states mirror the experimental arrangement implemented.
26. P. G. Kwiat, K. Mattle, H. Weinfurter, A. Zeilinger, A. V. Sergienko, and Y. Shih , "New High-Intensity Source of Polarization-Entangled Photon Pairs," Phys. Rev. Lett. **75**, 4337 (1995).
27. J. Svozilík, M. Hendrych, and J. P. Torres, "Bragg reflection waveguide as a source of wavelength-multiplexed polarization-entangled photon pairs," Opt. Express **20**, 15015–15023 (2012).
28. D. Kang and A. S. Helmy, "Generation of polarization entangled photons using concurrent type-I and type-0 processes in AlGaAs ridge waveguides," Opt. Lett. **37**, 1481–1483 (2012).
29. S. V. Zhukovsky, L. G. Helt, P. Abolghasem, D. Kang, J. E. Sipe, and A. S. Helmy, "Bragg reflection waveguides as integrated sources of entangled photon pairs," J. Opt. Soc. Am. B **29**, 2516–2523 (2012).

1. Introduction

Entanglement is not only a fundamental concept in Quantum Mechanics with profound implications, but also a basic ingredient of many recent technological applications that has been put forward in quantum communications and quantum computing [1, 2]. Entanglement is a very special type of correlation between particles that can exist in spite of how distant they are. Nevertheless, the term entanglement is sometimes also used to refer to certain correlations existing between different degrees of freedom of a single particle [3].

By and large, the most common method to generate photonic entanglement, that is entanglement between photons, is the process of spontaneous parametric down-conversion (SPDC) [4]. In SPDC, two lower-frequency photons are generated when an intense higher-frequency pump beam interacts with the atoms of a non-centrosymetric nonlinear crystal. Entanglement can reside in any of the degrees of freedoms that characterize light: angular momentum (polarization and orbital angular momentum), momentum and frequency, or in several of them, what is known as hyper-entanglement. Undoubtedly, polarization is the most widely used resource to generate entanglement between photons thanks to the existence of many optical elements to control the polarization of light and to the easiness of its manipulation when compared to other characteristics of a light beam, e.g., its spatial shape or bandwidth.

#186956 - $15.00 USD Received 13 Mar 2013; revised 12 Apr 2013; accepted 12 Apr 2013; published 26 Apr 2013

The implementation of entanglement-based photonic technologies should consider the development of high-efficient, compact, and highly tunable sources of entangled photons. High efficiency helps to reduce the pump power required to generate a high flux of down-converted photons, and broad tunability allows the preparation of different types of quantum states. Compactness makes possible to use the entanglement source under a greater variety of circumstances, such as, for instance, would be the case in free space applications [5]. Along these lines, the use of waveguides is very advantageous. Contrary to the case of SPDC in bulk crystals, where a very large number of spatial modes is generated, and only a few of them effectively contribute to the generated entangled state, the use of waveguides allows the reduction of the number of modes to a few guided modes [6], and, in this way, it contributes to enhance the overall efficiency of the nonlinear interaction [7].

The capability of integration of the SPDC source with other elements, such as the pumping laser or optical circuits, in a single platform, might be crucial for the implementation of entanglement-based quantum circuits in an out-of-the-lab environment. Semiconductor technologies are nowadays a mature technology that offers a myriad of possibilities, and that allows the fabrication of an integrated monolithic source of entangled photon pairs. Bragg reflection waveguides (BRWs) in $Al_xGa_{1-x}As$ could make possible the integration of all of these elements in a single semiconductor platform. In the last few years, different nonlinear optics processes have been observed experimentally in $Al_xGa_{1-x}As$ BRWs, such as second-harmonic generation [8, 9], difference-frequency generation [10] and spontaneous parametric down-conversion [11]. Also, BRWs have been demonstrated as edge-emitting diode lasers where the fundamental lasing mode is a photonic bandgap mode or a Bragg mode [12], and electrically pumped parametric fluorescence was demonstrated subsequently [13].

GaAs based waveguides show a broad transparency window ($1-17\ \mu$m), large damage threshold, low linear propagation loss and an extremely high non-linear coefficient [14]. In spite of GaAs being an isotropic material, not showing birefringence, phase-matching can nevertheless be reached between high frequency light propagating as a photonic bandgap mode, or Bragg mode, and low frequency light beams propagating as bound modes based on total-internal reflection (see Fig. 1) [15]. Fortunately, strong modal dispersion in BRWs offers significant control over the spectral width [16] and the type of spectral correlations [17] of the emitted photons.

In this paper, we demonstrate that the use of BRWs allows the generation of highly entangled pairs of photons in polarization via the observation of the violation of the Clauser-Horne-Shimony-Holt (CHSH) Bell-like inequality [18]. Bell's inequalities are a way to demonstrate entanglement [19], since the violation of a Bell's inequality makes impossible the existence of one joint distribution for all observables of the experiment, returning the measured experimental probabilities [20].

In a previous work [11], the existence of time-correlated paired photons generated by means of SPDC in BRWs was reported, but the existence, and quality, of the entanglement present was never explored. The generation of polarization entanglement in alternative semiconductor platforms has been demonstrated recently in a silicon-based wire waveguide [21], making use of four-wave mixing, a different nonlinear process to the one considered here, and in a AlGaAs semiconductor waveguide [22], where as a consequence of the opposite propagation directions of the generated down-converted photons, two type-II phase-matched processes can occur simultaneously.

2. Device description and SHG characterization

A schematic of the BRW used in the experiment is shown in Fig. 1. Grown on an undoped [001] GaAs substrate, the epitaxial structure has a three-layer waveguide core consisting of a 500 nm

#186956 - $15.00 USD Received 13 Mar 2013; revised 12 Apr 2013; accepted 12 Apr 2013; published 26 Apr 2013

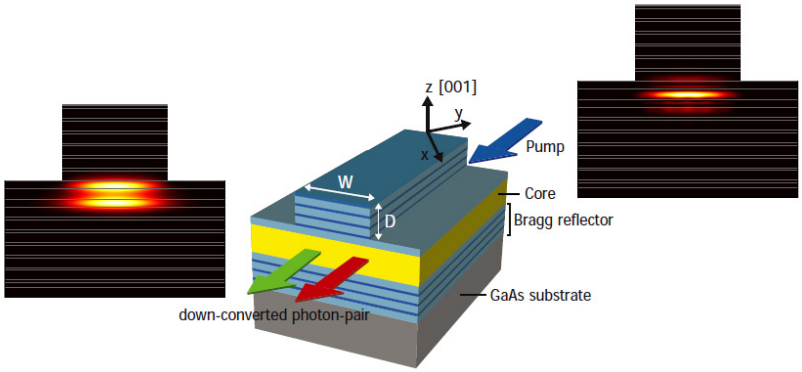

Fig. 1. Bragg reflection waveguide structure used to generate paired photons correlated in time and polarization (type-II SPDC) at the telecommunication window (1550 nm). The insets show the spatial shape of the pump mode that propagates inside the waveguide as a Bragg mode, and the spatial shape of the down-converted, which are modes guided by total internal reflection (TIR). W: width of the ridge; D: depth of the ridge.

thick $Al_{0.61}Ga_{0.39}As$ layer and a 375 nm $Al_{0.20}Ga_{0.80}As$ matching-layer on each side. These layers are sandwiched by two symmetric Bragg reflectors, with each consisting of six periods of 461 nm $Al_{0.70}Ga_{0.30}As$/129 nm $Al_{0.25}Ga_{0.65}As$. A detailed description of the epitaxial structure can be found in [23]. The wafer was then dry etched along [110] direction to form ridge waveguides with different ridge widths. The device under test has a ridge width of 4.4 μm, a depth of 3.6 μm and a length of 1.2 mm. The structure supports three distinct phase-matching schemes for SPDC, namely: type-I process where the pump is TM-polarized and the down-converted photon pairs are both TE-polarized; type-II process where the pump is TE-polarized while the photons of a pair have mutually orthogonal polarization states, and type-0 process where all three interacting photons are TM-polarized [14]. For the experiment here, we investigate type-II SPDC, which is the nonlinear process that produce the polarizations of the down-converted photons required to generate polarization entanglement. Since both photons show orthogonal polarizations, after traversing a non-polarizing beam splitter and introducing in advance an appropriate temporal delay between them, they can result in a polarization-entangled pair of photons.

During the fabrication process of the BRW, slight changes in the thickness and aluminium concentration of each layer result in small displacements of the actual phase-matching wavelength from the design wavelength. For this reason, we first use second harmonic generation (SHG) before examining SPDC to determine the pump phase-matching wavelength for which the different schemes (type-I, type-II or type-0) are more efficient.

The experimental arrangement for SHG is shown in Fig. 2(a). The wavelength of a single-frequency tunable laser (the fundamental beam) was tuned from 1545 nm to 1575 nm. An optical system shapes the light into a Gaussian-like mode, which is coupled into the BRW to generate the second harmonic beam by means of SHG. At the output, the power of the second harmonic wave is measured to determine the efficiency of the SHG process. Figure 2(b) shows the phase-matching tuning curve showing the dependency of generated second-harmonic power on the fundamental wavelength. From the figure, three resonance SH features could be resolved corresponding to the three supported phase-matching schemes. As mentioned earlier, the process of interest here is type-II. For this particular type of phase-matching, maximum efficiency takes place at the fundamental wavelength of 1555.9 nm. To generate the second

#186956 - $15.00 USD Received 13 Mar 2013; revised 12 Apr 2013; accepted 12 Apr 2013; published 26 Apr 2013

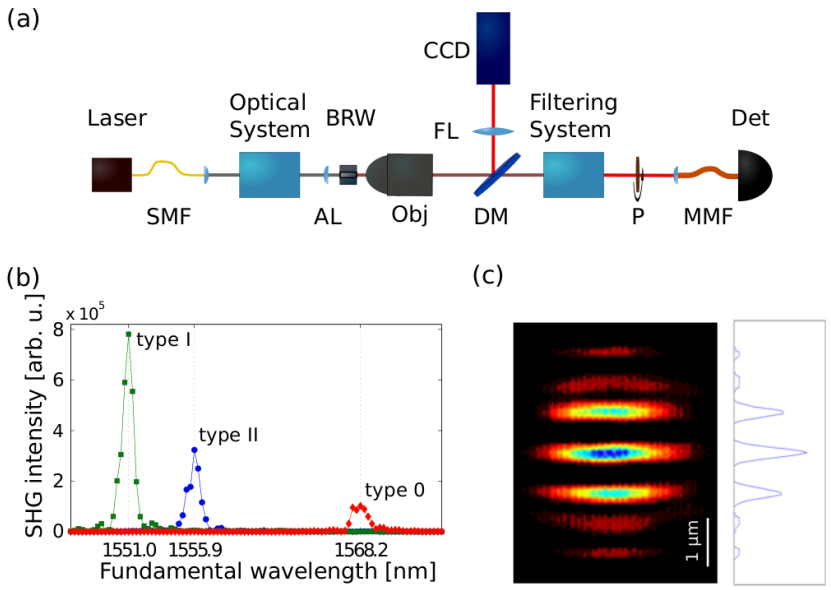

Fig. 2. (a) Experimental setup for SHG. The pump laser is a tunable external-cavity semiconductor laser (TLK-L1550R, Thorlabs). The Optical System consists of a linear power attenuator, polarization beam splitter and a half-wave plate. The Filtering System consists of a neutral density filter and low-pass filter. SMF: single-mode fiber; AL: aspheric lens; BRW: Bragg reflection waveguide; Obj: Nikon 50×; DM: dichroic mirror; FL: Fourier lens; CCD: Retiga EXi Fast CCD camera; P: polarizer; MMF: multi-mode fiber; Det: single-photon counting module (SPCM, PerkinElmer). (b) Phase-matching curve of the BRW as a function of the wavelength of the fundamental wave. (c) Beam profile of the Bragg mode of the second harmonic wave generated by means of the SHG process, captured with a CCD camera after imaging with a magnification optical system of 100× (Fourier lens with focal length f=400 mm).

harmonic beam by means of type-II SHG in Fig. 2(b), we use a half-wave plate to rotate the polarization of the fundamental light coming from the laser by 45-degrees, to generate the required fundamental beams with orthogonal polarizations.

In BRW, phase-matching takes place between different types of guided modes which propagate with different longitudinal wavevectors. The fundamental beam (around 1550 nm) corresponds to a total internal reflection (TIR) mode, and the second harmonic beam (around 775 nm) is a Bragg mode. The measured spatial profile of this Bragg mode is shown in Fig. 2(c).

3. Experimental set-up for the generation of polarization entanglement

The experimental setup used to generate polarization-entangled paired photons and the measurement of the Bell-like inequality violation is shown in Fig. 3(a). The pump laser is a tunable single-frequency diode laser with an external-cavity (DLX 110, Toptica Photonics) tuned to 777.95 nm. Light from the laser traverses an optical system, with an attenuator module, spatial filter and beam expander, in order to obtain a proper input beam. Even though the optimum option for exciting the pump Bragg mode would be to couple directly into the photonic bandgap mode using a spatial light modulator (SLM), the small feature size in the field profile of the Bragg mode and its oscillating nature imposed serious challenges for using an SLM. Therefore, we choose instead to pump the waveguide with a tightly focused Gaussian

#186956 - $15.00 USD Received 13 Mar 2013; revised 12 Apr 2013; accepted 12 Apr 2013; published 26 Apr 2013

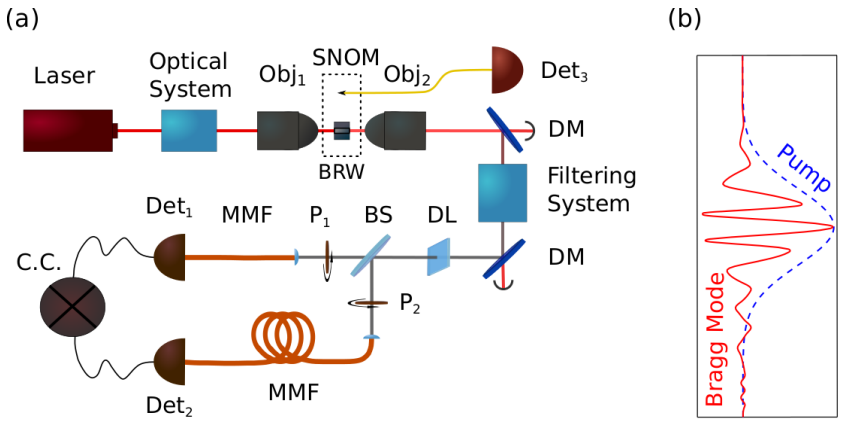

Fig. 3. (a) Experimental setup for SPDC. The Optical System is composed of a linear power attenuator, spatial filter and beam expander. SNOM: scanning near-field optical microscope probe; BRW: Bragg reflection waveguide; Objectives: Obj_1 (Nikon 100×) and Obj_2 (Nikon 50×); DM: dichroic mirror; Filtering System: 2 DMs, band-pass and long-pass filters; DL: delay line (birefringent plate); BS: beam splitter; P_1 and P_2: linear film polarizers; MMF: multi-mode fiber; D_1 and D_2: InGaAs single-photon counting detection modules; D_3: low-power silicon detector; C.C.: coincidence-counting electronics. (b) Amplitude profiles of the theoretical Bragg mode and the Gaussian-like pump beam.

pump beam (see Fig. 3(b)) with a waist of $\sim 1.5\ \mu$m, that is coupled into the waveguide using a 100× objective. Our calculations show that the estimated modal overlap between the Gaussian pump beam and the Bragg mode of the waveguide is around 20%, which should be added to the total losses of the system. A scanning near-field optical microscope (SNOM) probe was attached to the support of the BRW, in order to perform sub-micrometric 3D beam profile scans to maximize the coupling efficiency of the incident pump beam into the pump Bragg mode. The power of the laser light before the input objective was measured to be 13 mW. Taking into account the transmissivity of the objective for infrared light (70%), the transmissivity of the facet of the BRW (73%) and the calculated overlap between the laser light and the Bragg mode of the waveguide (around 20%), the estimated pump power available for SPDC process inside the waveguide is ~ 1.3 mW.

The generated down-converted photons are collected using a 50× objective and separated from the pump photons using four dichroic mirrors (DM), band-pass and long-pass filters. Each DM has a 99% transmissivity at the pump wavelength. The attenuation of the band-pass filter (45 nm FWHM bandwidth centered at 1550 nm) is 10^{-4}, and the long-pass filter (cut-on wavelength: 1500 nm) introduces an additional attenuation of 10^{-3} at the pump wavelength.

In general, photons propagating in a waveguide with orthogonal polarizations have different group velocities (group velocity mismatch, GVM), which in conjunction with non-negligible group velocity dispersion (GVD), result in different spectra for the cross-polarized photons [24]. As a consequence, the polarization and frequency properties of the photons are mixed. The two photons of a pair could be, in principle, distinguished by their time of arrival at the detectors, as well as their spectra, which diminishes the quality of polarization entanglement achievable. In order to obtain high-quality polarization entanglement, it is thus necessary to remove all the distinguishing information coming from the temporal/frequency degree of freedom. For this reason, the 45 nm band pass filter was applied to remove most of the distinguishing spectral information, and off-chip compensation was implemented with a delay line to remove arrival time information.

#186956 - $15.00 USD Received 13 Mar 2013; revised 12 Apr 2013; accepted 12 Apr 2013; published 26 Apr 2013

A quartz birefringent plate with a length of 1 mm, vertically tilted around 30° was used to introduce a 32 fs time delay between photons, which is experimentally found to be the optimum value to erase temporal distinguishing information caused by the group velocity mismatch (GVM) and the GVD. The calculated group velocities for TE and TM down-converted photons are 8.98×10^7 m/s and 9.01×10^7 m/s, respectively. The GVD parameter is $D\sim$ -7.9$\times10^2$ ps/(nm·km) for both polarizations. When considering these values of the GVM and GVD, our calculations show that the optimum delay for generating the highest degree of polarization entanglement is $\sim$ 31.2 fs, which agrees with the value obtained experimentally.

The down-converted photons are separated into arms 1 and 2 with a 50/50 beam splitter (BS) in order to generate a polarization-entangled two-photon state of the form

$$\left|\Psi^+\right\rangle = \frac{1}{\sqrt{2}}\left\{|H\rangle_1|V\rangle_2 + |V\rangle_1|H\rangle_2\right\}, \tag{1}$$

where $|H\rangle$ and $|V\rangle$ denote the two possible polarizations of the photons (horizontal and vertical), propagating in arms 1 or 2. Horizontal (vertical) photons corresponds to photons propagating inside the waveguide as TE (TM) mode. We neglect cases where both photons leave the BS through the same output port, by measuring only coincidences between photons propagating in arms 1 and 2 (post-selection), which implies that 50% of the generated pairs are not considered. Finally, to measure Bell's inequality violations, the entangled photons are projected into different polarization states with linear film polarizers, and coupled into multi-mode fibers connected to InGaAs single-photon detection modules (id201, idQuantique), where optical and electronic delays are introduced to measure coincidental events with time-to-amplitude converter (TAC) electronics. The coincidences window for all measurements was set to 3 ns.

4. Violation of the CHSH inequality

To obtain a first indication that the pairs of photons propagating in arms 1 and 2 are truly entangled in the polarization degree of freedom, so that their quantum state can be written of the form given by Eq. (1), one detects one of the photons, i.e., the photon propagating in arm 1, after projection into a specific polarization state $|\Psi\rangle_1 = \cos\theta_1|H\rangle_1 - \sin\theta_1|V\rangle_1$ [25], and measures in coincidence the remaining photon after projection into a set of polarization bases $|\Psi\rangle_2 = \cos\theta_2|V\rangle_2 + \sin\theta_2|H\rangle_2$, with θ_2 spanning from 0 to 2π [26]. Ideally, the coincidence counts as a function of θ_2 should follow the form of $\cos^2(\theta_1+\theta_2)$, which yields a visibility $V=(Max-Min)/(Max+Min)$ of 100%. Therefore, the highest the visibility measured, the highest the quality of the generated polarization-entangled state.

Figures 4(a) and (b) show the results of the measurements for two specific cases: $\theta_1 = 0°$ and $\theta_1 = 45°$. The measured visibility, subtracting the accidental coincidences, is 98% for $\theta_1 = 0°$, and to 91% for $\theta_1 = 45°$. Without subtraction of accidental coincidences, the corresponding measured visibility is 80% for $\theta_1 = 0°$ and 77% for $\theta_1 = 45°$. The accidental coincidences, with respect to the total number of events counted, were measured experimentally, introducing an electronic delay in the trigger of the second detector driving it out of the detection window of the first detector. The same electronic delay had to be introduced before the TAC electronics in order to have the coincidence events from the same amount of single events, but totally uncorrelated in this case. This technique made possible to measure the correct visibility of the fringes using the maximum efficiency detector settings, in order to obtain lower standard deviation of the measurements. The optimum trigger rate for this experiment was found to be 100 KHz, measuring an average of $3,550$ and $6,200$ photon counts per second in each detector, and a maximum flux rate of coincidences of 3 pairs of photons per second. The low trigger rate is one of the reasons for the observation of such a low flux rate of down-converted photons observed, since it implies that the detectors are closed most of the time. The detection window

#186956 - $15.00 USD Received 13 Mar 2013; revised 12 Apr 2013; accepted 12 Apr 2013; published 26 Apr 2013

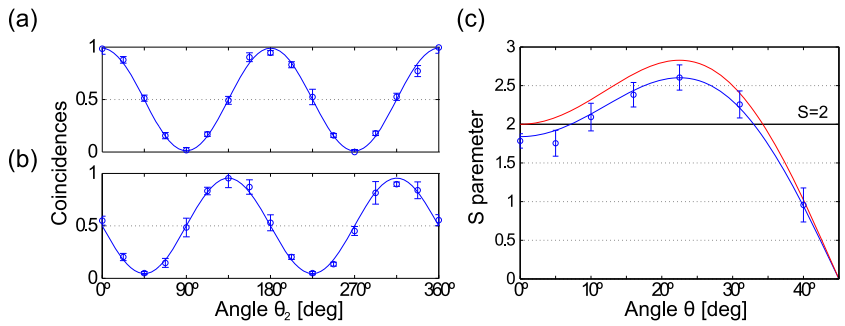

Fig. 4. Normalized coincidence measurements as a function of the polarization state of photon 2 when photon 1 is projected into a polarization state with: (a) $\theta_1 = 0^\circ$ and (b) $\theta_1 = 45^\circ$. The data shown in (a) and (b) is subtracting from the raw data the number of accidental coincidences. (c) Violation of the CHSH inequality. Parameter S as a function of the angle θ. The small blue circles with error bars represent the experimental data with their standard deviations. The blue solid curves in (a) and (b) are theoretical predictions assuming that the visibility is 98% in (a) and 91% in (b). The red (upper) curve in (c) is the theoretical prediction for S. The blue curve in (c) is the best fit. The inequality holds if $S \leq 2$. The maximum value attained is $S = 2.61 \pm 0.16$. The data shown in (c) is without subtraction of accidental coincidences.

for these measurements was set to 100 ns.

In a CHSH inequality experiment [18], one measures photon coincidences between photon 1, after being projected into a polarization state defined by angles θ_1 or θ_1', and photon 2, after a similar polarization projection defined by angles θ_2 or θ_2'. The CHSH inequality holds if

$$S = |E(\theta_1,\theta_2) - E(\theta_1,\theta_2') + E(\theta_1',\theta_2) + E(\theta_1',\theta_2')| \leq 2, \tag{2}$$

where

$$E(\theta_1,\theta_2) = \frac{C(\theta_1,\theta_2) + C(\theta_1^\perp,\theta_2^\perp) - C(\theta_1^\perp,\theta_2) - C(\theta_1,\theta_2^\perp)}{C(\theta_1,\theta_2) + C(\theta_1^\perp,\theta_2^\perp) + C(\theta_1^\perp,\theta_2) + C(\theta_1,\theta_2^\perp)} \tag{3}$$

and $\theta_{1,2}^\perp = \theta_{1,2} + 90^\circ$. Figure 4(c) shows the value of the parameter S as a function of the angle θ, where $\theta \equiv \theta_2 - \theta_1 = \theta_2' + \theta_1' = -\theta_2 - \theta_1'$, which attains the maximum possible violation, i.e., $S = 2\sqrt{2}$. For the ideal case, one would obtain $S(\theta) = 3\cos 2\theta - \cos 6\theta$, which is the red (upper) curve depicted in Fig. 4(c). Sixteen measurements were performed for each value of the angle θ. For the maximum inequality violation ($\theta = 22.5^\circ$), the polarizer settings were $\theta_1 = 0^\circ$, $\theta_1' = -45^\circ$, $\theta_2 = 22.5^\circ$ and $\theta_2' = 67.5^\circ$. In this case, we obtained a value of the inequality of $S = 2.61 \pm 0.16$, which represents a violation by more than 3 standard deviations. This represents a stronger violation of the CHSH inequality than previously reported [22] for a vertically pumped BRW structure, where the measured value was $S = 2.23 \pm 0.11$.

Regarding the measurements of the S parameter, no accidental coincidences were subtracted from the absolute measurement obtained. In order to increase the signal-to-noise ratio, the detection window in both detectors was decreased to 20% of its previous time duration (from 100 ns to 20 ns), having thus a corresponding decrease in total number of single and coincidence counts detected. Now, the measured average flux rate is 600 and 500 photon counts per second in each detector, and a maximum value of 0.3 pairs of photons per second.

To estimate the efficiency of the SPDC process, we take into account that the detection window is $\tau = 20$ ns, and the trigger rate of detection is 100 kHz. The efficiency of each single-photon detector is 25%. The pump power injected into the BRW waveguide is estimated to be

#186956 - $15.00 USD Received 13 Mar 2013; revised 12 Apr 2013; accepted 12 Apr 2013; published 26 Apr 2013

around 1.3 mW. Assuming that the transmissivity of each optical system, traversed by signal/idler photons, not including detection efficiency, is $\sim 10\%$, it results in an estimated SPDC efficiency of $\sim 10^{-10}$ in the filtering bandwidth.

5. Conclusions

We have demonstrated that polarization-entangled paired photons generated in a semiconductor Bragg reflection waveguide (BRW) show a visibility higher than 90% in all the bases measured, a requisite for obtaining high quality entanglement. It has also been experimentally demonstrated that the generated two-photon state clearly violate the CHSH inequality, and that the presented BRW source can be considered an expedient source of high-quality polarization-entangled two-photon states.

Alternative BRW configurations with no need of post-selection of down-converted photons can be implemented using, for instance, non-degenerate SPDC, where signal and idler photons bear different wavelengths [27], or concurrency of two conversion processes [28]. For this, one can make use of the great versatility offered by BRWs and design the layer structure to achieve phase-matching at the required wavelengths. Optimization of the generation rate of down-converted photons can be achieved by optimizing the layer thicknesses and Al concentrations, so that the mode overlap between photons at different wavelength increases. BRW made of AlGaAs can potentially offer higher generation rates than ferroelectrical waveguides made of PPLN or PPKTP, since they show a much higher second-order nonlinear coefficient. However, in practice, both the pump and the down-converted modes are subject to losses, chiefly by two processes: radiation losses, mainly in the Bragg modes, and scattering of light due to surface roughness [29]. Fortunately, improvements in design and fabrication of the BRW could reduce the losses of the pump and down-converted waves, increase mode overlap and enhance the coupling efficiency of the pump light into the pump mode that propagates in the waveguide.

It is important to note that the platform described and used here offers the unique possibility of integrating the pump laser with the nonlinear element to enable self-pumped on-chip generation of polarization entanglement, without the use of off-chip compensation and bandpass filtering, as is carried in this work. There are two theoretical proposals to achieve this aim, both use dispersion engineering of the BRWs. One uses type-II process in a BRW with zero-GVM [24], while the other one uses concurrent type-I and type-0 processes [28].

In combination with the development of quantum circuits composed of properly engineered arrays of waveguides, and the integration of the laser pump source in the same chip, our results show that semiconductor technology based on the use of BRW in $Al_xGa_{1-x}As$ is a promising path to develop integrated entanglement-based quantum circuits.

Acknowledgments

We would like to thank M. Micuda for his collaboration in certain stages of the experiment and R. de J. León-Montiel for useful discussions. This work was supported by Projects FIS2010-14831 and FET-Open 255914 (PHORBITECH). J. S. thanks the project FI-DGR 2011 of the Catalan Government. This work was also supported in part by projects CZ.1.05/2.1.00/03.0058 of the Ministry of Education, Youth and Sports of the Czech Republic and by PrF-2012-003 of Palacký University. P. Abolghasem, D. Kang and A. S. Helmy acknowledge the support of Natural Sciences and Engineering Research Council of Canada (NSERC) for funding this research and CMC Microsystems for growing the wafer. M. Hendrych is currently with Radiantis.

#186956 - $15.00 USD Received 13 Mar 2013; revised 12 Apr 2013; accepted 12 Apr 2013; published 26 Apr 2013